

ARTICLE TYPE**Accretion-induced collapse to third family compact stars as trigger for eccentric orbits of millisecond pulsars in binaries**David Edwin Alvarez-Castillo*¹ | John Antoniadis² | Alexander Ayriyan^{3,4} | David Blaschke^{1,5,6} | Victor Danchev⁷ | Hovik Grigorian^{3,4,8} | Noshad Khosravi Largani⁵ | Fridolin Weber^{9,10}¹Bogoliubov Laboratory for Theoretical Physics, Joint Institute for Nuclear Research, Joliot-Curie street 6, 141980 Dubna, Russia²Max-Planck-Institut für Radioastronomie and Argelander Institut für Astronomie, Auf dem Hügel 69, 53121 Bonn, Germany³Laboratory for Information Technologies, Joint Institute for Nuclear Research, Joliot-Curie street 6, 141980 Dubna, Russia⁴Computational Physics and IT Division, A.I. Alikhanyan National Science Laboratory, Alikhanyan Brothers street 2, 0036 Yerevan, Armenia⁵Institute of Theoretical Physics, University of Wrocław, Max Born place 9, 50-204 Wrocław, Poland⁶National Research Nuclear University (MEPhI), Kashirskoe Shosse 31, 115409 Moscow, Russia⁷Department of Physics, Sofia University St. Kliment Ohridski, 5 James Bourchier Blvd, 1164 Sofia, Bulgaria⁸Department of Physics, Yerevan State University, Alek Manukyan street 1, 0025 Yerevan, Armenia⁹Department of Physics, San Diego State University, 5500 Campanile Drive, San Diego, CA 92182, USA¹⁰Department of Physics, University of California, San Diego, La Jolla, CA 92093, USA**Correspondence**

*D. Alvarez-Castillo Email: sculkaputz@gmail.com

A numerical rotating neutron star solver is used to study the temporal evolution of accreting neutron stars using a multi-polytrope model for the nuclear equation of state named ACB5. The solver is based on a quadrupole expansion of the metric, but confirms the results of previous works, revealing the possibility of an abrupt transition of a neutron star from a purely hadronic branch to a third-family branch of stable hybrid stars, passing through an unstable intermediate branch. The accretion is described through a sequence of stationary rotating stellar configurations which lose angular momentum through magnetic dipole emission while, at the same time, gaining angular momentum through mass accretion. The model has several free parameters which are inferred from observations. The mass accretion scenario is studied in dependence on the effectiveness of angular momentum transfer which determines at which spin frequency the neutron star will become unstable against gravitational collapse to the corresponding hybrid star on the stable third-family branch. It is conceivable that the neutrino burst which accompanies the deconfinement transition may trigger a pulsar kick which results in the eccentric orbit. A consequence of the present model is the prediction of a correlation between the spin frequency of the millisecond pulsar in the eccentric orbit and its mass at birth.

KEYWORDS:

neutron star, accretion, binary systems

1 | INTRODUCTION

One of the most intriguing phenomena in compact star physics is the appearance of eccentric orbits in binaries of a millisecond pulsar (MSP) with a low-mass white dwarf in a rather

narrow region of orbital periods, see Fig. 1. In (J. Antoniadis, 2014) it has been demonstrated that the observed eccentricities of $e \simeq 0.01-0.15$ can be generated from the dynamical interaction of the binary with a circumbinary disc for periods between 15 and 50 days. P. C. C. Freire & Tauris (2014), however, proposed that these binary MSPs may form from the rotationally

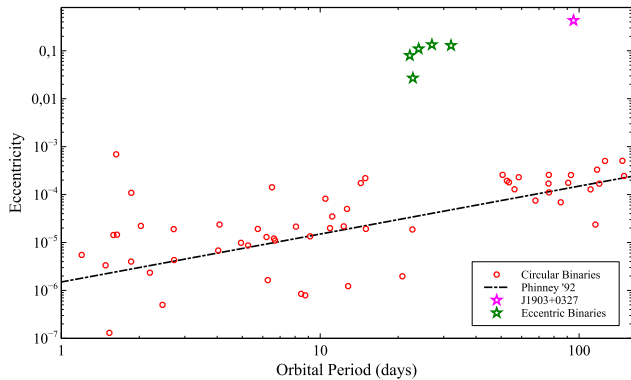


FIGURE 1 Eccentricity vs. orbital period for millisecond pulsars in binaries with white dwarf companions, see (J. Antoniadis, 2014; Stovall, 2019).

delayed accretion-induced collapse of a massive white dwarf. In J. Antoniadis et al. (2016) it has been shown that the companion star to one of these MSPs is indeed a low-mass white dwarf. In a recent work (Jiang, Li, Dey, & Dey, 2015) an accretion induced phase transition to a strange quark star has been suggested as an origin for the eccentricity of the orbit in the period range.

In this contribution we would like to explore a scenario of accretion onto a pulsar that may undergo a phase transition to a hybrid star with a quark matter core situated on a third family branch which thus involves a decent spin-up and structural reconfiguration of the compact star interior that may result in energy release by violent neutrino emission. The latter may result in the neutrino rocket mechanism that produces a compact star kick (see, e.g., (Berdermann, Blaschke, Grigorian, & Voskresensky, 2006; Peng, Zhang, Luo, & Chou, 2004; Sagert & Schaffner-Bielich, 2007)) as the origin for the eccentricity just in that window of orbital periods where mass transfer from a circumbinary disc is most effective.

In order to develop the scenario, we shall first consider a model for disc accretion that results in spin-up and mass increase of the compact star. We then suggest an equation of state (EoS) with a strong phase transition for the compact star matter fulfilling the criterion for the formation of a third-family branch of hybrid stars (Gerlach, 1968), separated from the one for ordinary neutron stars by a sequence of unstable configurations (Alford, Han, & Prakash, 2013). With such a setting one can suggest a prompt catastrophic rearrangement of the stellar structure as the origin for a compact star kick and thus an eccentric orbit. The EoS shall be chosen such that the modern constraints for the minimal maximum mass of $\sim 2 M_{\odot}$ for PSR J0740+6620 (Cromartie, n.d.) and the new NICER mass-radius constraints for PSR J0030+0451 will be fulfilled: $M = 1.44^{+0.15}_{-0.14} M_{\odot}$ and $R = 13.02^{1.24}_{1.06}$ km for three oval spots (Miller et al., 2019) as well as $M = 1.34^{+0.15}_{-0.16} M_{\odot}$ and

$R = 12.71^{1.14}_{1.19}$ km for one small hot spot and a azimuthally-extended narrow crescent (Riley et al., 2019). Moreover, the EoS should describe a pulsar at $1.4 M_{\odot}$ with a tidal deformability obeying the LIGO constraint $\Lambda_{1.4} = 190^{+390}_{120}$ (Abbott, 2018). Since the lowest well-measured mass for the eccentric MSPs in Fig. 1 is $1.353^{+0.014}_{0.017} M_{\odot}$ for PSR J2234+0611 (Stovall, 2019), the candidate EoS for the scenario should have in the static case an onset mass for the strong phase transition at or below this value.

2 | METHODOLOGY

The results presented in this paper are obtained with the authors' own numerical integrator of Einstein's field equation for rotating compact stars based on the Hartle and Thorne methodology (Hartle & Thorne, 1968), which consists of the development of a perturbation solution based on the Schwarzschild metric. The perturbed metric is expanded through second order in the star's rotational velocity, Ω , and is given by

$$ds^2 = -e^{\nu} \left[1 + 2(h_0 + h_2 P_2) \right] dt^2 + e^{\lambda} \left[1 + \frac{2(m_0 + m_2 P_2)}{r - 2M} \right] dr^2 + r^2 \left[1 + 2(v_2 - h_2) P_2 \right] \left[d\theta^2 + \sin^2(\theta) (d\phi - \omega dt)^2 \right] + O(\Omega^3), \quad (1)$$

where the functions $M(r)$ and $\lambda(r)$ are solutions of the Tolman-Oppenheimer-Volkoff (TOV) equation ($e^{\lambda} = (1 - 2M/r)^{-1}$), and $h_0(r)$, $m_0(r)$, $h_2(r)$, $m_2(r)$, and $v_2(r)$ denote monopole and quadrupole perturbation functions. The stellar deformation is described by the Legendre polynomial

$$P_2 = P_2(\cos \theta) = (3 \cos^2 \theta - 1)/2, \quad (2)$$

and $\omega(r)$ is the angular (frame-dragging) frequency relative to a static observer at spacelike infinity. The energy-momentum tensor is characterized by two more perturbation functions, $p_0^*(r)$ and $p_2^*(r)$, once again contributing to radial and θ -dependent perturbations (through P_2). The equations of all the perturbations can be readily derived from Einstein's field equations (Hartle & Thorne, 1968). The perturbation equations can be integrated by starting from the TOV solution by choosing a guess value for the angular velocity and fixing it through multiple integrations with the shooting method. The angular velocity for an inertial local observer $\bar{\omega}$ is obtained in this way. It is related to the angular frequency ω in (1) through $\bar{\omega} = \Omega - \omega$, where $\Omega = u^{\phi}/u^t$ is the star's angular velocity (defined by the 4-velocity components of a co-rotating observer). The asymptotics of the perturbation functions allow one to find them unambiguously for a given angular velocity Ω or angular momentum boundary value J .

The code is conceptually divided into a TOV integrator and a function which takes the TOV input and integrates all the perturbations radially outward with the corresponding boundary value settings (Hartle & Thorne, 1968). A 4th order Runge-Kutta method has been used due to its relative simplicity and accuracy. Several versions of the code were developed, one of which allowing us to determine the properties of stars with pre-defined baryon numbers (listed further down in the paper). In addition to the standard procedure of Hartle and Thorne, care has been taken to compute the proper mass shedding limit by taking into account the dragging of inertial frames as described in (Weber, 1999).

The model for matter accretion from a neutron star's disc is based on (Bejger, Fortin, Haensel, & Zdunik, 2011), considering the baryon mass M_b and angular momentum J to be the variables of such an evolution. A single star's evolution is seen as a set of stationary rotating configurations of different M_b and J values. Angular momentum can be gained from infalling particles and lost through the interaction between the star's magnetic field and the accretion disk. The relevant evolution equation is

$$\frac{dJ}{dM_b} = l_{\text{tot}} = \kappa l(r_0) - l_m, \quad (3)$$

where $l(r_0)$ is the specific angular momentum of the infalling particle at the innermost radius of the disc, r_0 , while l_m gives the magnetic torque divided by the accretion rate. The quantity κ describes the amount of angular momentum of the infalling particles which the star can actually receive. The value of κ is thus in the range of [0, 1]. The magnetic torque is given in terms of the dipole moment of the star, $\mu = BR^3$ as

$$l_m = \frac{\mu^2}{9r_0^3 \dot{M}_b} \left(3 - 2\sqrt{\frac{r_c^3}{r_0^3}} \right). \quad (4)$$

The inner disc radius is determined through a transcendental equation relating the magnetospheric radius r_m , the corotation radius r_c and the relativistic marginally stable orbit r_{ms} as follows

$$\frac{1}{\Omega r} \frac{dl}{dr} = \frac{1}{2} f_{ms}(r_0) = \left(\frac{r_m}{r_0} \right)^{7/2} \left(\sqrt{\frac{r_c^3}{r_0^3}} - 1 \right), \quad (5)$$

where the corresponding radii are given by

$$r_m = \frac{\mu^{4/7}}{(GM)^{1/7} \dot{M}_b^{2/7}}, \quad (6)$$

$$r_c = \left(\frac{GM}{\Omega^2} \right)^{1/3}, \quad (7)$$

$$0 = f_{ms}(r_{ms}). \quad (8)$$

Evolution through accretion is modelled by numerical integration of (3) which makes use of the boundary J for a given M_b integration of neutron star models to generate a sequence based on initial baryon mass and magnetic field values. The

results further down were obtained by preparing an array of J values and integrating (3) with the corresponding M_{b0} values and a given value of the angular momentum transfer coefficient κ . Last but not least, a decrease of the neutron star magnetic field has been considered through a simple phenomenological model in which the accreted mass M_{acc} "buries" the initial magnetic field B_i , described by

$$B(M_{acc}) = \frac{B_i}{1 + M_{acc}/m_B}. \quad (9)$$

This model was suggested by (Shibazaki, Murakami, Shaham, & Nomoto, 1989). It has a free parameter m_B which controls the speed at which the magnetic field decreases. Values of m_B based on observations are in the range $10^{-5} - 10^{-4} M_\odot$.

A final estimate on the time during which accretion takes place depends on the value of \dot{M}_b . It should be noted that the overall evolution is degenerate since the ratio μ^2/\dot{M}_b determines the RHS of Eq. (6). Changing the values of μ and \dot{M}_b simultaneously can lead to the same track if properly scaled, but the time in which the overall evolution takes place depends only on \dot{M}_b . For that reason, several different values of the initial magnetic field B_i and \dot{M}_b have been considered in the listed results to show the dependence on these quantities. All of them, however, are of the order of $\dot{M}_b \cong 10^{-9} M_\odot$, $B_i \cong 10^8$ G.

3 | EQUATION OF STATE

For the present study we will exploit an equation of state in the form of a multi-polytrope parametrisation as it can be found, e.g., in (Alvarez-Castillo & Blaschke, 2017; Hebel, Lattimer, Pethick, & Schwenk, 2013; Read, Lackey, Owen, & Friedman, 2009). It consists of piecewise polytrope regions in density that are joined thermodynamically consistently. For the lowest density parts that correspond to the outer NS crust ($n < 0.5n_0$) we implement the BPS EoS ((Baym, Pethick, & Sutherland, 1971)), to be followed by an intermediate phase of homogeneous matter in β -equilibrium ($0.5n_0 < n < 1.1n_0$). Above $1.1n_0$, we introduce four polytropic segments described by:

$$P(n) = \kappa_i (n/n_0)^{\Gamma_i}, \quad (10)$$

where $n_i < n < n_{i+1}$, $i = 1 \dots 4$ define the regions with constant κ_i and polytropic index Γ_i . Since $P(n) = n^2(d(\epsilon(n)/n))/(dn)$, the remaining thermodynamical variables can be easily determined (Zdunik, Bejger, Haensel, & Gourgoulhon, 2006):

$$\epsilon(n)/n = \frac{1}{n_0^{\Gamma_i}} \int dn \kappa n^{\Gamma_i-2} = \frac{1}{n_0^{\Gamma_i}} \frac{\kappa n^{\Gamma_i-1}}{\Gamma_i-1} + C, \quad (11)$$

$$\mu(n) = \frac{P(n) + \epsilon(n)}{n} = \frac{1}{n_0^{\Gamma_i}} \frac{\kappa \Gamma_i}{\Gamma_i-1} n^{\Gamma_i-1} + m_0, \quad (12)$$

where C is fixed by the condition $\epsilon(n \rightarrow 0) = m_0 n$. The above equations can be recast into the following forms:

$$n(\mu) = \left[n_0^{\Gamma_i} (\mu - m_0) \frac{\Gamma_i - 1}{\kappa \Gamma_i} \right]^{1/(\Gamma_i - 1)}, \quad (13)$$

$$P(\mu) = \kappa \left[n_0^{\Gamma_i} (\mu - m_0) \frac{\Gamma_i - 1}{\kappa \Gamma_i} \right]^{\Gamma_i / (\Gamma_i - 1)}, \quad (14)$$

which are suitable for performing a Maxwell construction of a first-order phase transition between the hadron and quark phases. Each of the polytropic regions has physical meaning. The first one is defined as the result of a fit to the stiffest EoS version provided in (Hebeler et al., 2013). We are interested in an EoS with a strong first order phase transition that would produce a large jump in energy density $\Delta\epsilon$ at the critical pressure P_c in order to fulfill the Seidov criterion (Seidov, 1971) for a gravitational instability: $\Delta\epsilon > (\epsilon_c + 3P_c)/2$. Therefore we define the second polytrope as a region of constant pressure $P_c = \kappa_2$ ($\Gamma_2 = 0$), which can result from a Maxwell construction using (14) for the neighboring regions. The remaining polytropes, in the regions $i = 3, 4$, at the highest densities beyond the first order phase transition shall correspond to stiff quark matter. It shall be sufficiently stiff to result in stable hybrid star configurations with a maximum mass of at least $2 M_\odot$, thus fulfilling the constraint from the lower bound of the 2σ region of PSR J0740+6620 (Cromartie, n.d.), and similar constraints stemming from PSR J0348+0432 (J. et. al. Antoniadis, 2013) and PSR J1614-2230 (Demorest, Pennucci, Ransom, Roberts, & Hessels, 2010).

TABLE 1 EOS for the ACB5 (Paschalidis et al., 2018). The functional form of the polytrope is defined by Eq. (10) in the main text. The first polytrope ($i = 1$) is fitted to the nuclear EoS at supersaturation densities, the second one ($i = 2$) describes a first-order phase transition with constant pressure $P_c = \kappa_2$ and $\Gamma_2 = 0$ in the $n_2 < n < n_3$ region. The polytropes that lie in regions 3 and 4, i.e., above the phase transition represent high-density matter, e.g., quark matter. Maximum masses M_{\max} on the hadronic and hybrid branches correspond to region 1 and 4. The minimal mass M_{\min} on the hybrid branch lies in region 3 and marks the onset of the third family solution.

i	Γ_i	κ_i [MeV/fm ³]	n_i [1/fm ³]	$m_{0,i}$ [MeV]	$M_{\max/\min}$ [M_\odot]
1	4.777	2.1986	0.1650	939.56	1.40
2	0.0	33.969	0.2838	939.56	–
3	4.000	0.4373	0.4750	995.03	1.39
4	2.800	2.7919	0.7500	932.48	2.00

As it has been noted in (Alvarez-Castillo & Blaschke, 2017), it is rather challenging to find a parametrisation with only one polytrope for the high-density region that would obey thermodynamic consistency and at the same time provide a high maximum mass without violating the causality constraint on the squared speed of sound $c_s^2 = dP/d\epsilon < 1$. The multi-polytrope parametrisation has also proven successful for analyses of the compactness constraint that follows from the recent measurements of tidal deformability (Abbott, 2018) (see also (De et al., 2018; Zhao & Lattimer, 2018)) of compact stars in the mass range around $1.36 M_\odot$ by analysing the gravitational wave signal from the inspiral phase of the binary merger GW170817 (Annala, Gorda, Kurkela, & Vuorinen, 2018; Paschalidis et al., 2018) and by placing constraints on the EoS (Miller, Chirenti, & Lamb, 2019).

The four-polytrope model which was introduced in (Paschalidis et al., 2018) and denoted there as "ACB5" fulfills the present constraints from multimessenger astronomy on maximum mass and compactness of compact stars (given at the end of the Introduction) and has recently also been studied concerning its behaviour under fast rotation (Blaschke et al., 2019; Bozzola, Espino, Lewin, & Paschalidis, 2019). In Table 1 we provide the parameters of this EoS.

4 | RESULTS, DISCUSSION AND PERSPECTIVES

We have utilized our rotating neutron star solver in order to obtain solutions for the axially symmetric solutions of the Einstein equations with the EoS ACB5. On this basis we studied the spin and mass evolution of the compact star within the accretion scenario defined in Section 2 in dependence on the effectiveness of angular momentum transfer, as described also in (Bejger, Blaschke, Haensel, Zdunik, & Fortin, 2017) for a similar case.

In Fig. 2 we show the baryon mass versus equatorial radius for given angular momenta $J = 0.05, 0.1, 0.15, \dots, 0.45 J_0$, with $J_0 = GM_\odot^2/c$ (blue solid lines), together with the static case (black solid line) and the Keplerian limit (red solid line). In order to guide the eye we have shown also a few lines of constant baryon mass which allow to estimate the path of a collapsing star from the edge of the hadronic branch to the corresponding point on the stable hybrid star branch (third family) under simultaneous conservation of angular momentum and baryon mass. We want to note that for the present type of EoS such a catastrophic rearrangement of the stellar interior is possible, in principle, at the free-fall time scale. In previous works on quark deconfinement in accreting low-mass binaries (Glendenning, Pei, & Weber, 1997) this was not the case and the rearrangement would have taken a secular time scale of about

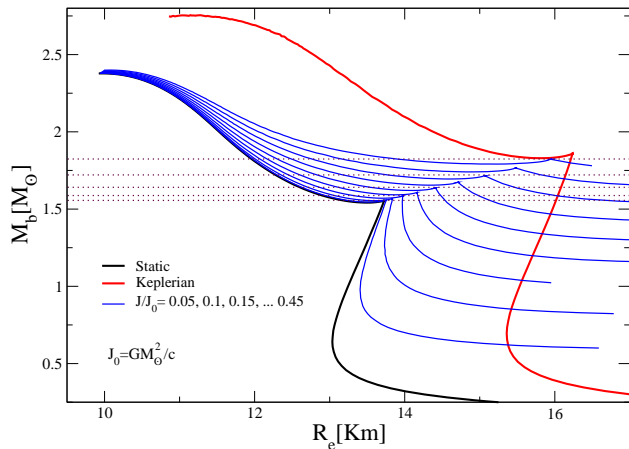


FIGURE 2 Baryon mass versus equatorial radius for the ACB5 EoS. Static configurations are black solid lines, the Keplerian limit is shown as red solid line. Blue solid curves are at constant angular momentum J . The maroon horizontal dotted lines of constant baryon mass can guide the eye to follow from an endpoint of stability on the hadronic branch to a point on the hybrid star branch which would be reached by a collapse under simultaneous conservation of angular momentum J and baryon mass M_b . For the gravitational mass of these hybrid star configurations, see the light green curve in Fig. 3 .

$10^6 - 10^8$ yr in order to get rid of the angular momentum difference by, e.g., electromagnetic dipole radiation. However, such a direct transition scenario would also entail that the orbits would re-circularize quite fastly (on a scale of $\sim 10^3$ yrs) due to mass-accretion and/or tidal forces. The collapse to a hybrid star as an origin for the eccentric MSP orbit in the prompt collapse scenario should therefore have occurred rather recently.

Alternatively, in order to circumvent the problem with re-circularization in the prompt collapse scenario, one can discuss a delayed collapse scenario on the basis of the calculation presented in Fig. 3 . If the binary star gains mass by accretion but fails to reach the onset mass for the transition when the accretion and spin-up process stops, it could then undergo a spin-down evolution and thus reach the instability line for transition to a hybrid star configuration by loss of angular momentum. There are several realisations of this process, depending on the period of the binaries: a) short period binaries which would always reach the maximum mass during accretion, resulting in circular orbits, b) long period binaries that would collapse only after spin-down, producing eccentric orbits, and c) very long period binaries that would never undergo the transition.

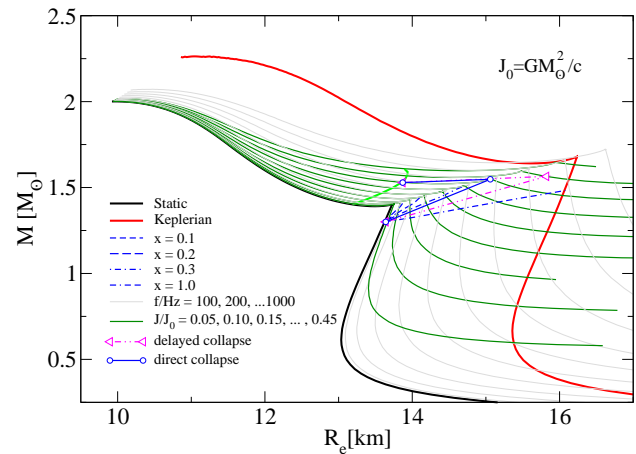


FIGURE 3 Gravitational mass versus equatorial radius for the ACB5 EoS. Static configurations are black solid lines, the Keplerian limit is shown as red solid line. Green curves are at constant angular momentum J and grey lines are for constant rotation frequency $f = 1/P$, where P is the period. The light green curve connects those points on the hybrid star branches which can be reached by a collapse from the maximum of stability on the hadronic branch under conservation of angular momentum J and baryon mass M_b , see Fig. 2 . The blue lines with different styles indicate evolution trajectories that stars take in this diagram according to the accretion model describes in the text, for different efficiencies x of angular momentum transfer. The solid blue line corresponds to direct collapse while the magenta dash-double-dotted line shows the path for delayed collapse.

In Fig. 3 we show the gravitational mass versus equatorial radius for the same ACB5 EoS and for the same grid of fixed angular momenta (green solid lines). The light grey lines are curves of fixed spin frequency $f = 100, 200, \dots, 1000$ Hz. The blue lines with different styles are the trajectories that a pulsar takes under mass accretion during the low-mass X-ray binary phase for given effectiveness x of the angular momentum transfer in this process. Once the trajectory reaches the line that joins the endpoints of stability of hadronic star configurations, the collapse sets in which transforms the hadronic star into a hybrid star, with a birth mass on the light green line. We note that for a very effective angular momentum transfer (e.g., $x = 1$) the star would never reach to the line for the onset of collapse. It would instead continue the spin-up process until it goes over to the so-called propeller regime.

In Fig. 4 we show as the black solid line the final result of this work, the correlation between frequency and mass of the spun-up MSP that is kicked into an eccentric orbit by

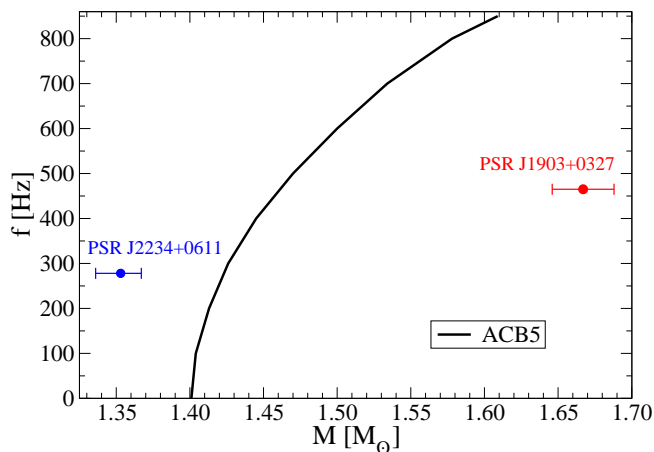


FIGURE 4 Spin frequency versus gravitational mass of the hybrid star at its birth in the accretion induced collapse from a neutron star. The black solid line shows the result of our model for the ACB5 EoS. Of the few known millisecond pulsars in eccentric orbits (see Fig. 1) we show those for which mass and spin are precisely measured: PSR J2234+0611 (Stovall, 2019) and PSR J1903+0327 (P. C. C. Freire, 2011). They confirm the trend of the present model: larger mass entails higher spin frequency.

a strong phase transition, here described by the model EoS ACB5. We note that this result is strongly EoS dependent and could thus serve as a diagnostic tool for determining the state of matter in compact stars. In particular, the lower limit of the curve depends on the onset mass of the phase transition for the static configuration as a solution of the Tolman-Oppenheimer-Volkoff equations. Here, a lower onset mass for the third-family branch (and thus the so-called mass twins) could be provided, e.g., by the hybrid star EoS on the basis of the generalized nonlocal NJL model EoS for color superconducting developed in (Alvarez-Castillo, Blaschke, Grunfeld, & Pagura, 2019) guided by the density-functional based quark matter EoS for the relativistic string-flip model of (Kaltenborn, Bastian, & Blaschke, 2017). For such an EoS it would be no problem to match the data point for PSR J2234+0611 (Stovall, 2019) also shown in that figure.

It should be noted that the high-mass pulsar PSR J1903+0327 has a highly debated origin (P. C. C. Freire, 2011) and should probably not be considered to belong to the population of the other eccentric MSPs shown in Fig. 1 since its companion is not a low-mass white dwarf but rather a main sequence star and its orbital period of 95.2 days is beyond the range of 15 - 50 days for the other eccentric MSPs. In order to put our scenario for the origin of the eccentric MSPs to the

test, we look forward to precise mass measurements, in particular for highly spun-up pulsars like PSR J0955-6150 with a spin period of 2.0 ms (Octau et al., 2018).

For the present scenario it is not immediately obvious how more massive eMSPs could be explained like PSR J1946+3417 (Barr et al., 2017) with a precisely determined high mass of $1.828(22) M_{\odot}$. It is, however, also possible to develop the present scenario further so that another major structural rearrangement contributing to a pulsar kick may take place, even leading from a third to a fourth family, see (Alford & Sedrakian, 2017; Li, Sedrakian, & Alford, 2019).

Acknowledgements

We acknowledge the Russian Science Foundation for supporting the part of the work on phenomenology of compact stars with strong first order phase transition under grant number 17-12-01427. The work of F.W. was supported by the National Science Foundation (USA) under Grant PHY-1714068.

REFERENCES

- Abbott, B. P. et al. 2018, *Phys. Rev. Lett.*, **121**(16), 161101.
- Alford, M. G., Han, S., & Prakash, M. 2013, *Phys. Rev.*, **D88**(8), 083013.
- Alford, M. G., & Sedrakian, A. 2017, *Phys. Rev. Lett.*, **119**(16), 161104.
- Alvarez-Castillo, D. E., & Blaschke, D. B. 2017, *Phys. Rev.*, **C96**(4), 045809.
- Alvarez-Castillo, D. E., Blaschke, D. B., Grunfeld, A. G., & Pagura, V. P. 2019, *Phys. Rev.*, **D99**(6), 063010.
- Annala, E., Gorda, T., Kurkela, A., & Vuorinen, A. 2018, *Phys. Rev. Lett.*, **120**(17), 172703.
- Antoniadis, J., Kaplan, D. L., Stovall, K. et al. 2016, *The Astrophysical Journal*, **830**, 36. doi:
- Antoniadis, J. et al. 2013, *Science*, **340**, 1233232.
- Antoniadis, J. 2014, *Astrophys. J. Letters*, **797**, L24.
- Barr, E. D., Freire, P. C. C., Kramer, M. et al. 2017, *Mon. Not. Roy. Astron. Soc.*, **465**(2), 1711-1719.
- Baym, G., Pethick, C., & Sutherland, P. 1971, *Astrophys. J.*, **170**, 299-317.
- Bejger, M., Blaschke, D., Haensel, P., Zdunik, J. L., & Fortin, M. 2017, *Astron. Astrophys.*, **600**, A39.
- Bejger, M., Fortin, M., Haensel, P., & Zdunik, J. L. 2011, *Astron. Astrophys.*, **536**, A87.
- Berdermann, J., Blaschke, D., Grigorian, H., & Voskresensky, D. N. 2006, *Prog. Part. Nucl. Phys.*, **57**, 334-342.
- Blaschke, D., Alvarez-Castillo, D. E., Ayriyan, A., Grigorian, H., Largani, N. K., & Weber, F. 2019, *Astrophysical aspects of general relativistic mass twin stars*, arXiv:1906.02522 [astro-ph.HE].
- Bozzola, G., Espino, P. L., Lewin, C. D., & Paschalidis, V. 2019, *Eur. Phys. J.*, **A55**(9), 149.
- Cromartie, H. T. et al. 2019, *Nature Astron.*, **3**, 439.
- De, S., Finstad, D., Lattimer, J. M., Brown, D. A., Berger, E., & Biwer, C. M. 2018, *Phys. Rev. Lett.*, **121**(9), 091102.

- Demorest, P., Pennucci, T., Ransom, S., Roberts, M., & Hessels, J. 2010, *Nature*, **467**, 1081-1083.
- Freire, P. C. C., & Tauris, T. M. 2014, *Monthly Notices of the Royal Astronomical Society*, **438**, L86-L90.
- Freire, P. C. C. et al. 2011, *Mon. Not. Roy. Astron. Soc.*, **412**, 2763.
- Gerlach, U. H. 1968, *Phys. Rev.*, **172**, 1325-1330.
- Glendenning, N. K., Pei, S., & Weber, F. 1997, *Phys. Rev. Lett.*, **79**, 1603-1606.
- Hartle, J. B., & Thorne, K. S. 1968, *Astrophys. J.*, **153**, 807.
- Hebeler, K., Lattimer, J. M., Pethick, C. J., & Schwenk, A. 2013, *Astrophys. J.*, **773**, 11.
- Jiang, L., Li, X.-D., Dey, J., & Dey, M. 2015, *Astrophys. J.*, **807**(1), 41.
- Kaltenborn, M. A. R., Bastian, N.-U. F., & Blaschke, D. B. 2017, *Phys. Rev.*, **D96**(5), 056024.
- Li, J. J., Sedrakian, A., & Alford, M. 2019, *Relativistic hybrid stars with sequential first-order phase transitions and heavy-baryon envelopes*, arXiv:1911.00276 [astro-ph.HE].
- Miller, M. C., Chirenti, C., & Lamb, F. K. 2019, *Constraining the equation of state of high-density cold matter using nuclear and astronomical measurements*, arXiv:1904.08907[astro-ph.HE].
- Miller, M. C., et al. 2019, *Astrophys. J. Lett.*, **887**, L24.
- Octau, F., Cognard, I., Guillemot, L., Tauris, T. M., Freire, P. C. C., Desvignes, G., & Theureau, G. 2018, *Astron. Astrophys.*, **612**, A78.
- Paschalidis, V., Yagi, K., Alvarez-Castillo, D., Blaschke, D. B., & Sedrakian, A. 2018, *Phys. Rev.*, **D97**(8), 084038.
- Peng, Q.-H., Zhang, L.-D., Luo, X.-L., & Chou, C.-K. 2004, *IAU Symp.*, **218**, 33.
- Read, J. S., Lackey, B. D., Owen, B. J., & Friedman, J. L. 2009, *Phys. Rev.*, **D79**, 124032.
- Riley, T. E., et al. 2019, *Astrophys. J. Lett.*, **887**, L21.
- Sagert, I., & Schaffner-Bielich, J. 2007, *Astron. Astrophys.*.
- Seidov, Z. 1971, *Sov. Astron.*, **15**, 347.
- Shibazaki, N., Murakami, T., Shaham, J., & Nomoto, K. 1989, *Nature*, **342**, 656-658.
- Stovall, K. et al. 2019, *Astrophys. J.*, **870**(2), 74.
- Weber, F. 1999, *Pulsars as astrophysical laboratories for nuclear and particle physics*, IoP, Bristol.
- Zdunik, J. L., Bejger, M., Haensel, P., & Gourgoulhon, E. 2006, *Astron. Astrophys.*, **450**, 747-758.
- Zhao, T., & Lattimer, J. M. 2018, *Phys. Rev.*, **D98**(6), 063020.

